

Implications of the cosmic infrared background for light production and the star formation history in the Universe

R. Gispert^{†*}, G. Lagache, and J.L. Puget

Institut d'Astrophysique Spatiale, Bât. 121, Université Paris XI, F-91405 Orsay Cedex

Abstract. The Cosmic Background due to the integrated radiation from galaxies over the whole life of the Universe is reviewed. We find that this background is well constrained by measurements. The total power in the background is in the range 60-93 nWm⁻²sr⁻¹. The data show the existence of a minimum separating the direct stellar radiation from the infrared part due to radiation reemitted by dust. This reemitted dust radiation is about 1-2.6 time the background power in the optical/near-IR thus much larger than the same ratio measured locally (30%). The far-infrared and submillimeter background is likely to be dominated by redshifted infrared galaxies. The long wavelength spectrum of the background being significantly flatter than the spectrum of these galaxies it strongly constrains the far-infrared radiation production rate history which must increase by a factor larger than 10 between the present time and a redshift 1 and then stays rather constant at higher redshift, contrary to the ultraviolet radiation production rate which decreases rapidly.

Several models of galaxy evolution have been proposed to explain the submillimeter background. In this paper we do not propose a new model; we systematically explore the allowed range of evolution histories allowed by the data. If infrared galaxies are mostly powered by starbursts as indicated by recent observations, this infrared production history reflects the history of star formation in the Universe.

1. Introduction

The history of star formation in the Universe is one of the key function in physical cosmology. It is closely linked to galaxy formation and evolution and controls the second most important contribution to the cosmic electromagnetic background after the Cosmic Microwave Background (CMB) generated at the time of recombination

Send offprint requests to: G. Lagache, lagache@ias.fr

* Richard Gispert died in the final stages of the preparation of this paper in August 1999.

at a redshift around 1000. It has been pointed out many times in the past 30 years, that measurements of the cosmic background radiated by all galaxies over the history of the Universe would be extremely valuable for physical cosmology. It would strongly constrain models for galaxy formation and evolution (see for example Partridge & Peebles, 1967). This background is expected to be composed of three main components:

- The stellar radiation in galaxies concentrated in the ultra-violet and visible with a redshifted component in the near InfraRed (IR)
- A fraction of the stellar radiation absorbed by dust either in the galaxies or in the intergalactic medium
- The radiation from active galactic nuclei (a fraction of which is also absorbed by dust and reradiated in the far-IR).

The energy in the first two components is derived from nucleosynthesis in stars, the last one probably derived from gravitational energy of accreted matter onto massive black holes. In the last two years the cosmic background at visible, IR and submillimeter (submm) wavelengths has been finally constrained by very deep source counts and upper limits on the diffuse isotropic emission at shorter wavelengths, and measured in the submm range. We review the observational situation in Sect. 2. In Sect. 3, we define the formalism of the determination of the IR radiation production rate history. When the spectrum of the sources dominating the background is strongly peaked around a wavelength of 80 μ m, the radiation production rate as a function of redshift can be directly inferred from the spectrum of the cosmic background. In Sect. 4, the sources of Cosmic Far-IR BackgRound (CFIRB) and their spectra are reviewed. In the likely hypothesis of this background being dominated by IR galaxies (either starburst galaxies or dust enshrouded AGNs), we derive the IR radiation production rate as a function of redshift in the Universe (Sect. 5). We compare it with other means to measure the star formation rate in Sect. 6.

The study presented here is different from the many studies of this type based on a model for Spectral Energy

Distribution (SED) and evolution of IR galaxies which, after some adjustments, account for the Cosmic Background. Considering the diversity of SED which can be used and the observational uncertainties it is clear that a range of histories of the IR galaxies is possible. The goal of this paper and of the method presented here is to explore systematically the range of possible solutions by a careful analysis of possible SEDs taking properly into account the observational uncertainties. The method developed in this paper is the only one so far to answer this question.

2. The Cosmic Background Radiation: observations

We summarise here the observational situation of the cosmic background which is the main observation used in this study. The values of the cosmic background at all wavelengths are discussed in Appendix 1 and shown on Fig. 1. We can compute the energy contained in the background above and below $6 \mu\text{m}$ using the best fits presented on Fig. 1. We obtain:

$$- E(<6 \mu\text{m})=E(\text{opt})= 2.4.1 \cdot 10^{-8} \text{ W m}^{-2} \text{ sr}^{-1}$$

$$- E(>6 \mu\text{m})=E(\text{FIR})= 4.5.2 \cdot 10^{-8} \text{ W m}^{-2} \text{ sr}^{-1}$$

We know that for local galaxies the ratio $E(\text{FIR})/E(\text{opt})$ is about 0.3 (Soifer & Neugebauer, 1991). We measure here a higher ratio which is about 1-2.6. This higher ratio results from two combined effects. First, the redshift effect will bring the light from optical to IR and thus will give more energy in the IR than for local galaxies. Nevertheless this effect cannot account for an IR to optical ratio much larger on average than the value observed today. This higher ratio can only be explained by a change of properties of galaxies that are making the background in the optical and the IR. A very simple comparison supports this idea: the energy in the background at $15 \mu\text{m}$ and in the optical domain is nearly the same. But the background at $15 \mu\text{m}$ in the Hubble Deep Field is made by a very small number of objects as compared to the number of sources which contribute to the bulk of the energy observed in the optical (Aussel et al. 1999). This means that the background in the IR is probably dominated by few objects with high IR luminosities. Thus these objects are not the standard IR counterparts of normal spiral and irregular galaxies.

3. Formalism of the determination of the radiation production rate history in the Universe

For a Universe following a Robertson-Walker metric with total density Ω_0 , and a cosmological constant Ω_Λ , the differential contribution dE to the background energy density (monochromatic or integrated over frequency, per unit volume) generated around redshift z during time dt is:

$$dE = \frac{\varphi(z)}{(1+z)} dt \quad (1)$$

where φ is the comoving energy production rate per unit volume at redshift z (note that here φ is not the spectral energy density).

The background spectral intensity (brightness per solid angle and frequency interval) I_ν is such that:

$$\nu I_\nu = \frac{c}{4\pi} \varphi(z) \left| \frac{dt}{dz} \right|_{1+z=\frac{\nu'}{\nu}} \quad (2)$$

where we assume a monochromatic spectrum for the sources radiating at frequency $\nu' = \nu(1+z)$ where ν is the observed frequency. In that case (δ function spectrum for the emitting objects), $\varphi(z)$ can be simply deduced from the background spectrum νI_ν (see Appendix 2).

The relations given above can be easily generalised to the case where the sources radiate through a broad spectrum:

$$\nu I_\nu = \frac{c\nu}{4\pi} \int_{\nu'=\nu}^{\infty} N_z L_{\nu'} \left| \frac{dt}{dz} \right| d\nu' \quad (3)$$

with N_z the number of sources per Mpc^3 and $L_{\nu'}$ the luminosity of the galaxies (in W/Hz).

$L_{\nu'}$ is the average over a large volume of SED of luminous IR galaxies which have been shown to dominate the $15 \mu\text{m}$ background at $z \simeq 0.7$ (Aussel et al 1999). The range of SED for IR galaxies are discussed in Sect. 4. The important result of this discussion is that all the far-IR SEDs of luminous IR galaxies are not very dependent of the energy source (starburst or dust enshrouded AGN) and varies slowly with the luminosity (Maffei, 1994; Guiderdoni 1998).

The unknown quantity in Eq. (3) becomes N_z . The full range of allowed functions for the number density of sources as a function of z is derived using Monte Carlo simulations for a set of IR galaxy spectra which covers the range of possible ones and for different cosmological models. The number density multiplied by the total luminosity of each model galaxy gives the IR luminosity density φ in function of z :

$$\varphi(z) = N_z \int_{\nu_0} L_{\nu_0} d\nu_0 \quad (4)$$

$\varphi(z)$ depends on the cosmological model via the $\frac{dt}{dz}$.

4. Sources of the Cosmic Background and their spectra

To determine $\varphi(z)$, we need to establish the range of acceptable average SEDs ($L_{\nu'}$) of the sources that are making the background.

¹ We can note that $\varphi(z) \times \frac{dt}{dz}$ is independent of the cosmological model. We nevertheless choose to use $\varphi(z)$ rather $\varphi(z) \times \frac{dt}{dz}$ as $\varphi(z)$ corresponds at $z=0$ to a measured value.

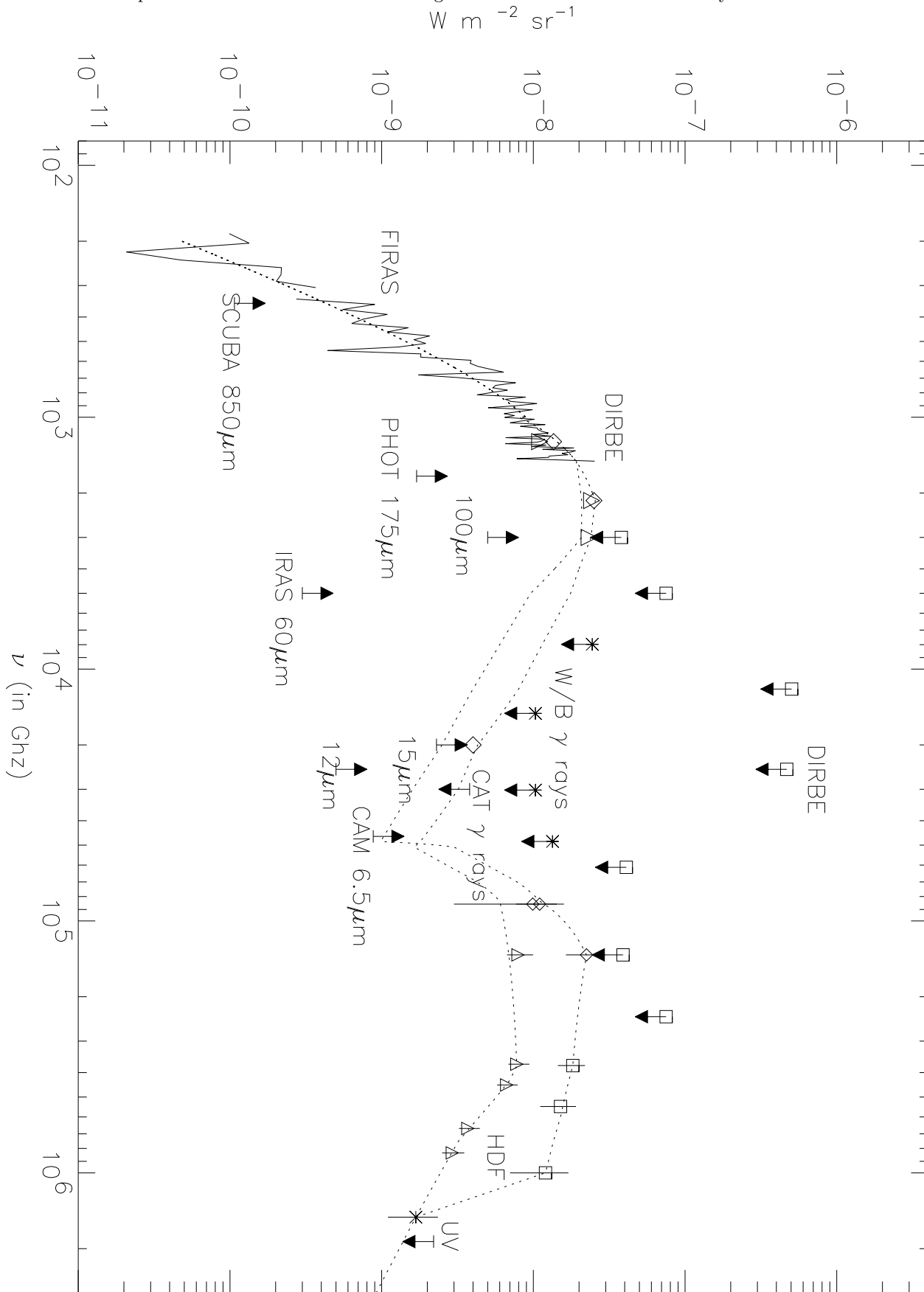


Fig. 1. Cosmic Background from the UV to the millimeter wavelength. In the UV domain, the upper limit is from Martin et al. (1991) and the value from Armand et al. (1994); the optical and near-IR points are from Pozzetti et al., 1998 (triangles) and Bernstein et al., in preparation (squares); The 3.5 and 2.2 μm points are from Dwek & Arendt (1998) and Gorjian et al. (2000); Squared upper limits are from Hauser et al. (1998) and crossed upper limits from Biller et al. (1998); the upper limit "CAT" is from Barrau (1998) and Barrau et al., in preparation; The 6.5 (Désert, private communication), 12 (Clements et al. 1999) and 15 μm (Elbaz et al. 1999) lower limits come from ISOCAM number counts; the value at 15 μm (\diamond) is an extrapolation of the counts using the Guiderdoni et al. (1998) model. At longer wavelength, we have the 100, 140 and 240 μm Lagache et al. 2000 (Δ) and Hauser et al. 1998 (\diamond) DIRBE values, lower limit from Dwek et al. (1998), upper limits from number counts at 60 (Lonsdale et al. 1990), 175 (Puget et al. 1999) and 850 μm (Barger et al. 1999). Dotted lines are an attempt to draw continuous

Table 1. Co-moving luminosity density φ derived from the CFIRB for the three galaxy model luminosities, the four dust spectral indexes and the three cosmologies (defined by Ω_Λ and Ω_0). Numbers on the right side of each row correspond to the minimal and maximal value of φ compatible with the CFIRB. The Hubble constant is the same for all cases ($h=0.65$). Given in column 10 is the χ^2 of the CFIRB “fit” derived from the luminosity density compared to the FIRAS and DIRBE measured values.

Log(L), α , Ω_Λ , Ω_0	Luminosity density φ (L_\odot/Mpc^3)								χ^2
	z=0.4	z=0.8	z=1.2	z=1.9	z=2.7	z=4.8	z=8		
12.5, 2.0, 0.0, 0.3	8.94 10 ⁸ 8.28 10 ⁶	1.15 10 ⁹ 9.14 10 ⁹	1.53 10 ⁹ 2.08 10 ⁹	1.26 10 ⁹ 1.85 10 ⁹	1.43 10 ⁹ 1.95 10 ⁹	6.68 10 ⁸ 1.23 10 ⁹	3.82 10 ⁸ 7.07 10 ⁸	0.054	
12.5, 2.0, 0.7, 0.3	6.36 10 ⁸ 1.01 10 ¹⁰	1.54 10 ⁹ 9.14 10 ⁹	1.91 10 ⁹ 2.59 10 ⁹	1.86 10 ⁹ 2.53 10 ⁹	2.01 10 ⁹ 2.96 10 ⁹	1.14 10 ⁹ 2.11 10 ⁹	5.64 10 ⁸ 1.21 10 ⁹	0.053	
12.5, 2.0, 0.0, 1.0	3.02 10 ⁸ 8.20 10 ⁹	1.36 10 ⁹ 1.85 10 ⁹	1.96 10 ⁹ 2.67 10 ⁹	1.73 10 ⁹ 2.54 10 ⁹	2.06 10 ⁹ 2.81 10 ⁹	1.04 10 ⁹ 2.07 10 ⁹	6.75 10 ⁸ 1.25 10 ⁹	0.053	
11.7, 2.0, 0.0, 0.3	1.50 10 ⁹ 7.52 10 ⁹	1.37 10 ⁹ 1.72 10 ⁹	1.49 10 ⁹ 2.19 10 ⁹	1.17 10 ⁹ 1.71 10 ⁹	1.25 10 ⁹ 1.70 10 ⁹	4.15 10 ⁸ 9.64 10 ⁸	3.82 10 ⁸ 5.19 10 ⁸	0.057	
11.7, 2.0, 0.7, 0.3	1.17 10 ⁹ 9.57 10 ⁹	1.84 10 ⁹ 2.39 10 ⁹	2.03 10 ⁹ 2.64 10 ⁹	1.71 10 ⁹ 2.22 10 ⁹	1.82 10 ⁹ 2.37 10 ⁹	7.46 10 ⁸ 1.64 10 ⁹	4.35 10 ⁸ 8.39 10 ⁸	0.057	
11.7, 2.0, 0.0, 1.0	5.24 10 ⁸ 6.38 10 ⁹	1.75 10 ⁹ 2.28 10 ⁹	1.96 10 ⁹ 2.54 10 ⁹	1.65 10 ⁹ 2.15 10 ⁹	1.79 10 ⁹ 2.33 10 ⁹	7.34 10 ⁸ 1.42 10 ⁹	4.62 10 ⁸ 8.91 10 ⁸	0.056	
10.8, 2.0, 0.0, 0.3	6.61 10 ⁸ 5.67 10 ⁹	2.11 10 ⁹ 2.66 10 ⁹	1.65 10 ⁹ 2.42 10 ⁹	1.14 10 ⁹ 1.68 10 ⁹	1.06 10 ⁹ 1.44 10 ⁹	3.72 10 ⁸ 8.01 10 ⁸	2.15 10 ⁸ 3.97 10 ⁸	0.065	
10.8, 2.0, 0.7, 0.3	7.88 10 ⁸ 9.57 10 ⁹	2.69 10 ⁹ 3.39 10 ⁹	2.26 10 ⁹ 3.31 10 ⁹	1.61 10 ⁹ 2.36 10 ⁹	1.56 10 ⁹ 2.12 10 ⁹	5.62 10 ⁸ 1.21 10 ⁹	3.65 10 ⁸ 6.75 10 ⁸	0.065	
10.8, 2.0, 0.0, 1.0	1.04 10 ⁹ 5.74 10 ⁹	2.48 10 ⁹ 3.23 10 ⁹	2.13 10 ⁹ 2.77 10 ⁹	1.55 10 ⁹ 2.31 10 ⁹	1.50 10 ⁹ 1.96 10 ⁹	5.81 10 ⁸ 1.12 10 ⁹	3.49 10 ⁸ 6.74 10 ⁸	0.062	
12.5, 1.7, 0.0, 0.3	9.48 10 ⁸ 7.53 10 ⁹	1.29 10 ⁹ 1.62 10 ⁹	1.52 10 ⁹ 2.06 10 ⁹	1.27 10 ⁹ 1.73 10 ⁹	1.30 10 ⁹ 1.76 10 ⁹	4.92 10 ⁸ 1.06 10 ⁹	3.32 10 ⁸ 5.69 10 ⁸	0.054	
12.5, 1.7, 0.7, 0.3	2.58 10 ⁹ 1.20 10 ¹⁰	1.54 10 ⁹ 2.10 10 ⁹	2.01 10 ⁹ 2.73 10 ⁹	1.76 10 ⁹ 2.58 10 ⁹	1.81 10 ⁹ 2.66 10 ⁹	8.55 10 ⁸ 1.71 10 ⁹	4.78 10 ⁸ 9.53 10 ⁸	0.051	
12.5, 1.7, 0.0, 1.0	4.31 10 ⁸ 7.37 10 ⁹	1.54 10 ⁹ 2.09 10 ⁹	2.02 10 ⁹ 2.73 10 ⁹	1.72 10 ⁹ 2.52 10 ⁹	1.86 10 ⁹ 2.53 10 ⁹	8.18 10 ⁸ 1.63 10 ⁹	5.25 10 ⁸ 9.71 10 ⁸	0.054	
11.7, 1.7, 0.0, 0.3	1.03 10 ⁹ 6.51 10 ⁹	1.60 10 ⁹ 2.01 10 ⁹	1.59 10 ⁹ 2.16 10 ⁹	1.17 10 ⁹ 1.71 10 ⁹	1.11 10 ⁹ 1.51 10 ⁹	3.78 10 ⁸ 8.14 10 ⁸	2.69 10 ⁸ 2.26 10 ⁸	0.060	
11.7, 1.7, 0.7, 0.3	8.92 10 ⁸ 8.35 10 ⁹	2.11 10 ⁹ 2.75 10 ⁹	2.12 10 ⁹ 2.75 10 ⁹	1.64 10 ⁹ 2.14 10 ⁹	1.61 10 ⁹ 2.10 10 ⁹	6.37 10 ⁸ 1.23 10 ⁹	3.82 10 ⁸ 7.38 10 ⁸	0.059	
11.7, 1.7, 0.0, 1.0	1.22 10 ⁹ 6.77 10 ⁹	1.90 10 ⁹ 2.47 10 ⁹	2.03 10 ⁹ 2.47 10 ⁹	1.60 10 ⁹ 2.08 10 ⁹	1.61 10 ⁹ 2.09 10 ⁹	6.07 10 ⁸ 1.34 10 ⁹	4.21 10 ⁸ 7.13 10 ⁸	0.057	
10.8, 1.7, 0.0, 0.3	8.92 10 ⁸ 5.63 10 ⁹	2.43 10 ⁹ 3.05 10 ⁹	1.71 10 ⁹ 2.70 10 ⁹	1.13 10 ⁹ 1.66 10 ⁹	9.98 10 ⁸ 1.36 10 ⁹	3.17 10 ⁸ 6.83 10 ⁸	1.72 10 ⁸ 3.17 10 ⁸	0.069	
10.8, 1.7, 0.7, 0.3	2.28 10 ⁹ 8.40 10 ⁹	2.77 10 ⁹ 3.77 10 ⁹	2.45 10 ⁹ 3.60 10 ⁹	1.50 10 ⁹ 2.38 10 ⁹	1.40 10 ⁹ 1.90 10 ⁹	5.11 10 ⁸ 1.10 10 ⁹	2.90 10 ⁸ 5.35 10 ⁸	0.065	
10.8, 1.7, 0.0, 1.0	1.06 10 ⁹ 5.73 10 ⁹	2.86 10 ⁹ 3.60 10 ⁹	2.27 10 ⁹ 3.33 10 ⁹	1.54 10 ⁹ 2.26 10 ⁹	1.41 10 ⁹ 1.91 10 ⁹	4.90 10 ⁸ 1.06 10 ⁹	3.07 10 ⁸ 2.90 10 ⁸	0.066	
12.5, 1.5, 0.0, 0.3	1.31 10 ⁹ 9.80 10 ⁹	1.25 10 ⁹ 1.70 10 ⁹	1.62 10 ⁹ 2.20 10 ⁹	1.24 10 ⁹ 1.81 10 ⁹	1.19 10 ⁹ 1.75 10 ⁹	4.28 10 ⁸ 9.22 10 ⁸	3.13 10 ⁸ 4.60 10 ⁸	0.058	
12.5, 1.5, 0.7, 0.3	8.95 10 ⁸ 8.38 10 ⁹	1.82 10 ⁹ 2.37 10 ⁹	2.09 10 ⁹ 2.71 10 ⁹	1.70 10 ⁹ 2.21 10 ⁹	1.86 10 ⁹ 2.42 10 ⁹	6.58 10 ⁸ 1.45 10 ⁹	4.90 10 ⁸ 2.99 10 ⁸	0.057	
12.5, 1.5, 0.0, 1.0	5.64 10 ⁸ 6.02 10 ⁹	1.73 10 ⁹ 2.25 10 ⁹	1.99 10 ⁹ 2.59 10 ⁹	1.66 10 ⁹ 2.46 10 ⁹	1.77 10 ⁹ 2.30 10 ⁹	7.22 10 ⁸ 1.39 10 ⁹	4.60 10 ⁸ 7.79 10 ⁸	0.056	
11.7, 1.5, 0.0, 0.3	1.26 10 ⁹ 5.86 10 ⁹	1.68 10 ⁹ 2.12 10 ⁹	1.72 10 ⁹ 2.52 10 ⁹	1.10 10 ⁹ 1.74 10 ⁹	1.09 10 ⁹ 1.49 10 ⁹	3.22 10 ⁸ 7.48 10 ⁸	2.46 10 ⁸ 3.61 10 ⁸	0.065	
11.7, 1.5, 0.7, 0.3	1.35 10 ⁹ 7.90 10 ⁹	2.28 10 ⁹ 2.87 10 ⁹	2.19 10 ⁹ 2.98 10 ⁹	1.59 10 ⁹ 2.33 10 ⁹	1.55 10 ⁹ 2.11 10 ⁹	5.50 10 ⁸ 1.19 10 ⁹	3.52 10 ⁸ 6.02 10 ⁸	0.061	
11.7, 1.5, 0.0, 1.0	1.10 10 ⁹ 6.91 10 ⁹	2.05 10 ⁹ 2.66 10 ⁹	2.11 10 ⁹ 2.74 10 ⁹	1.57 10 ⁹ 2.34 10 ⁹	1.53 10 ⁹ 2.00 10 ⁹	5.01 10 ⁸ 1.10 10 ⁹	4.24 10 ⁸ 2.99 10 ⁸	0.060	
10.8, 1.5, 0.0, 0.3	1.40 10 ⁹ 9.65 10 ⁹	2.60 10 ⁹ 3.27 10 ⁹	1.79 10 ⁹ 2.84 10 ⁹	1.07 10 ⁹ 1.70 10 ⁹	9.61 10 ⁸ 1.31 10 ⁹	2.62 10 ⁸ 6.25 10 ⁸	1.81 10 ⁸ 2.87 10 ⁸	0.070	
10.8, 1.5, 0.7, 0.3	1.08 10 ⁹ 7.33 10 ⁹	3.40 10 ⁹ 4.28 10 ⁹	2.53 10 ⁹ 3.72 10 ⁹	1.59 10 ⁹ 2.34 10 ⁹	1.37 10 ⁹ 1.87 10 ⁹	4.54 10 ⁸ 9.78 10 ⁸	2.77 10 ⁸ 4.74 10 ⁸	0.071	
10.8, 1.5, 0.0, 1.0	1.03 10 ⁹ 5.58 10 ⁹	3.16 10 ⁹ 3.98 10 ⁹	2.39 10 ⁹ 3.51 10 ⁹	1.53 10 ⁹ 2.25 10 ⁹	1.38 10 ⁹ 1.87 10 ⁹	4.26 10 ⁸ 9.18 10 ⁸	2.91 10 ⁸ 4.62 10 ⁸	0.069	
12.5, 1.3, 0.0, 0.3	1.69 10 ⁹ 7.85 10 ⁹	1.39 10 ⁹ 1.89 10 ⁹	1.57 10 ⁹ 2.31 10 ⁹	1.20 10 ⁹ 1.76 10 ⁹	1.16 10 ⁹ 1.58 10 ⁹	3.86 10 ⁸ 8.32 10 ⁸	2.07 10 ⁸ 4.12 10 ⁸	0.057	
12.5, 1.3, 0.7, 0.3	1.16 10 ⁹ 8.34 10 ⁹	1.93 10 ⁹ 2.51 10 ⁹	2.14 10 ⁹ 2.78 10 ⁹	1.69 10 ⁹ 2.20 10 ⁹	1.67 10 ⁹ 2.17 10 ⁹	6.12 10 ⁸ 1.35 10 ⁹	4.03 10 ⁸ 8.22 10 ⁸	0.057	
12.5, 1.3, 0.0, 1.0	1.23 10 ⁹ 7.32 10 ⁹	1.76 10 ⁹ 2.35 10 ⁹	2.07 10 ⁹ 2.77 10 ⁹	1.61 10 ⁹ 2.28 10 ⁹	1.66 10 ⁹ 2.35 10 ⁹	5.52 10 ⁸ 1.24 10 ⁹	4.70 10 ⁸ 8.63 10 ⁸	0.056	
11.7, 1.3, 0.0, 0.3	1.57 10 ⁹ 7.30 10 ⁹	1.76 10 ⁹ 2.39 10 ⁹	1.73 10 ⁹ 2.54 10 ⁹	1.13 10 ⁹ 1.65 10 ⁹	9.44 10 ⁸ 1.39 10 ⁹	3.29 10 ⁸ 7.10 10 ⁸	1.79 10 ⁸ 3.06 10 ⁸	0.063	
11.7, 1.3, 0.7, 0.3	1.42 10 ⁹ 8.30 10 ⁹	2.46 10 ⁹ 3.10 10 ⁹	2.32 10 ⁹ 3.15 10 ⁹	1.57 10 ⁹ 2.31 10 ⁹	1.49 10 ⁹ 2.02 10 ⁹	4.87 10 ⁸ 1.05 10 ⁹	3.19 10 ⁸ 5.46 10 ⁸	0.063	
11.7, 1.3, 0.0, 1.0	1.28 10 ⁹ 6.82 10 ⁹	2.23 10 ⁹ 2.81 10 ⁹	2.21 10 ⁹ 3.13 10 ⁹	1.54 10 ⁹ 2.30 10 ⁹	1.46 10 ⁹ 2.06 10 ⁹	4.74 10 ⁸ 1.06 10 ⁹	3.11 10 ⁸ 5.22 10 ⁸	0.061	
10.8, 1.3, 0.0, 0.3	1.47 10 ⁹ 5.52 10 ⁹	2.81 10 ⁹ 3.54 10 ⁹	1.95 10 ⁹ 3.08 10 ⁹	1.11 10 ⁹ 1.66 10 ⁹	8.85 10 ⁸ 1.25 10 ⁹	2.28 10 ⁸ 5.42 10 ⁸	1.64 10 ⁸ 2.45 10 ⁸	0.071	
10.8, 1.3, 0.7, 0.3	1.63 10 ⁹ 8.17 10 ⁹	3.70 10 ⁹ 4.65 10 ⁹	2.63 10 ⁹ 3.86 10 ⁹	1.58 10 ⁹ 2.32 10 ⁹	1.35 10 ⁹ 1.84 10 ⁹	3.69 10 ⁸ 8.58 10 ⁸	2.66 10 ⁸ 4.21 10 ⁸	0.072	
10.8, 1.3, 0.0, 1.0	8.68 10 ⁸ 3.66 10 ⁹	3.50 10 ⁹ 4.41 10 ⁹	2.53 10 ⁹ 4.00 10 ⁹	1.56 10 ⁹ 2.33 10 ⁹	1.30 10 ⁹ 1.83 10 ⁹	3.75 10 ⁸ 8.39 10 ⁸	2.73 10 ⁸ 4.08 10 ⁸	0.072	

Locally Soifer & Neugebauer (1991) have studied the population of IR galaxies at low redshift using the IRAS all sky survey. They have established the integrated IR luminosity per unit volume in the Universe today, its SED, the luminosity function of IR galaxies and the SED as a function of the integrated IR luminosity. The IR luminosity function shows two main components. One is associated with normal spiral galaxies which radiate a fraction of their energy in the IR (our Galaxy for example radi-

ates about one third of its luminosity in the IR). These galaxies are expected to have a luminosity function similar to the luminosity function of galaxies in the optical. However, the IR luminosity function does not show an exponential cut off like optical galaxies but display a power law behaviour at high luminosities: $\frac{dN}{dL} = L^{-2}$. This is also shown by more recent compilations of the IR luminosity functions (Sanders & Mirabel, 1996). This shows that the very luminous IR galaxies cannot be the IR counterpart of

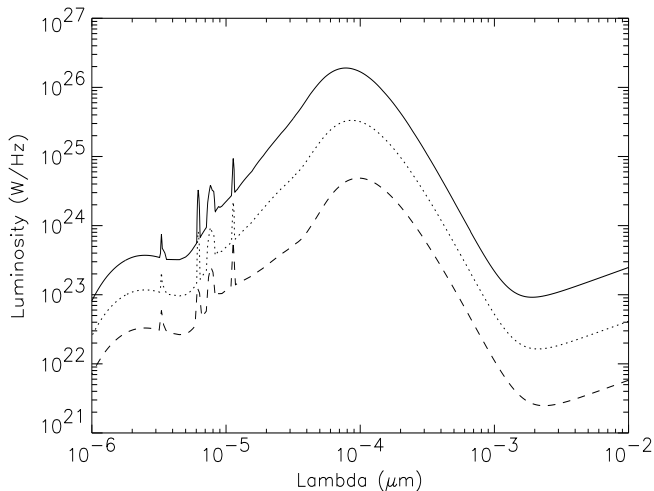


Fig. 2. Typical spectra of starburst galaxies (Maffei, 1994) for different luminosities (continuous line: $3 \cdot 10^{12} L_{\odot}$, dotted line: $5 \cdot 10^{11} L_{\odot}$, dashed line: $7 \cdot 10^{10} L_{\odot}$) with a spectral dust emission index in the far-IR of 2.

optical galaxies. In fact they have been shown to be starburst galaxies often associated with merging or interacting systems and for which the ratio of IR to optical luminosity increases with the bolometric luminosity (Sanders & Mirabel, 1996; Fang et al. 1998). One can thus conjecture that the luminosity function of mergers and interacting galaxies is very different from the luminosity function of normal galaxies. Using this rough separation, locally the relative contributions of starburst to normal galaxies is less than 10%. The integrated luminosity of normal galaxies is dominated by L_{\star} optical galaxies ($L_{IR\star} \simeq 10^{10} L_{\odot}$) whereas the integrated luminosity of IR starburst is dominated by galaxies with $L_{IR} \sim 10^{11} L_{\odot}$ (see for example Sanders & Mirabel, 1996).

26 of the galaxy detected by ISOCAM in the HDF north are identified with galaxies with known redshifts. Aussel (1999) has shown that the IR galaxies have luminosities greater than $3 \cdot 10^{10} L_{\odot}$ at $8.5 \mu\text{m}$ (in the rest frame) with a median redshift of 0.75, and thus bolometric luminosities between 1 and $3 \cdot 10^{11} L_{\odot}$. These galaxies, identified mostly as interacting systems or spiral galaxies, are luminous IR galaxies undergoing a starburst phase.

Spectra of IR galaxies have been modeled by Maffei (1994), using the observational correlation of the IRAS flux ratio 12/60, 25/60 and 60/100 with the IR luminosity (Soifer & Neugebauer, 1991). Examples of spectra for three different luminosities are shown in Fig. 2. The luminous IR galaxies are emitting more than 95% of their energy in the far-IR. Taking only such kind of galaxies obviously fails to reproduce the optical Extragalactic Background (EB). That is why we concentrate hereafter only on the far-IR part of the EB (the so-called Cosmic Far-IR Background, CFIRB).

It is possible however that part of the CFIRB energy might be due to dust enshrouded Active Galactic Nuclei (AGNs) for which the far-IR SED is very similar to starburst galaxies of similar luminosity. Based on the assumptions that 10% of the mass accreting into black hole is turned into energy and that the black hole masses measured in the HDF (Ford et al. 1998) are typical of galaxies, the AGN background energy would be in order of 10% of that from stars (Eales et al. 1999). These calculations are highly uncertain but are supported by the recent work of Almaini et al. (1999). The SEDs of high-redshift dust enshrouded AGNs are similar to those observed locally, and one can explain 10-20 % of the CFIRB. Because of the similar far-IR SEDs, the question of the fraction of the CFIRB due to AGNs is not relevant to the determination of the IR radiation production history. The estimates mentioned above are only important because they indicate that the IR radiation production history is likely to reflect the star formation history. Locally the average far-IR SED adjusted on the IRAS data (Soifer & Neugebauer, 1991) is well represented by the SED of a $8 \cdot 10^{10} L_{\odot}$ IR galaxy. As we have seen, at $z \sim 0.7$ the mid IR production is dominated by galaxies typically 2.5 times more luminous. Finally at higher redshift the main indication comes from the SCUBA deep surveys and also indicates an average SED dominated by ultraluminous IR galaxies. To take into account the uncertainty on the average far-IR SED, we use for the determination of the IR radiation production history, the SEDs from Maffei (1994) for galaxies with luminosities $7 \cdot 10^{10} L_{\odot}$, $5 \cdot 10^{11} L_{\odot}$ and $3 \cdot 10^{12} L_{\odot}$ which takes into account the change in the peak emission wavelength with luminosity. For the long wavelength behaviour, we allow the dust emissivity index of the model to vary from 1.3 to 2 which covers generously the uncertainty on this parameter for the average SED.

5. Luminosity density history from Monte Carlo simulations

5.1. The CFIRB spectrum

We used the CFIRB determination as described in Lagache et al. (2000). The CFIRB resulting from an integral over a significant redshift range is expected to be a smooth function of frequency. Therefore, we use a smooth fit for the determination of $\varphi(z)$. The CFIRB spectrum, can be fitted between 200 and $2000 \mu\text{m}$ by a modified Planck function as given by:

$$I(\nu) = 8.80 \times 10^{-5} (\nu/\nu_0)^{1.4} P_{\nu}(13.6K) \quad (5)$$

where $\nu_0 = 100 \text{ cm}^{-1}$. The set of parameters (T , τ , α) has been determined by a χ^2 minimization. The spectrum is sampled at 10 FIRAS frequency. The uncertainties on each sampled frequency are obtained by varying parameters until χ^2 is increased by 10%. In addition to the FIRAS data,

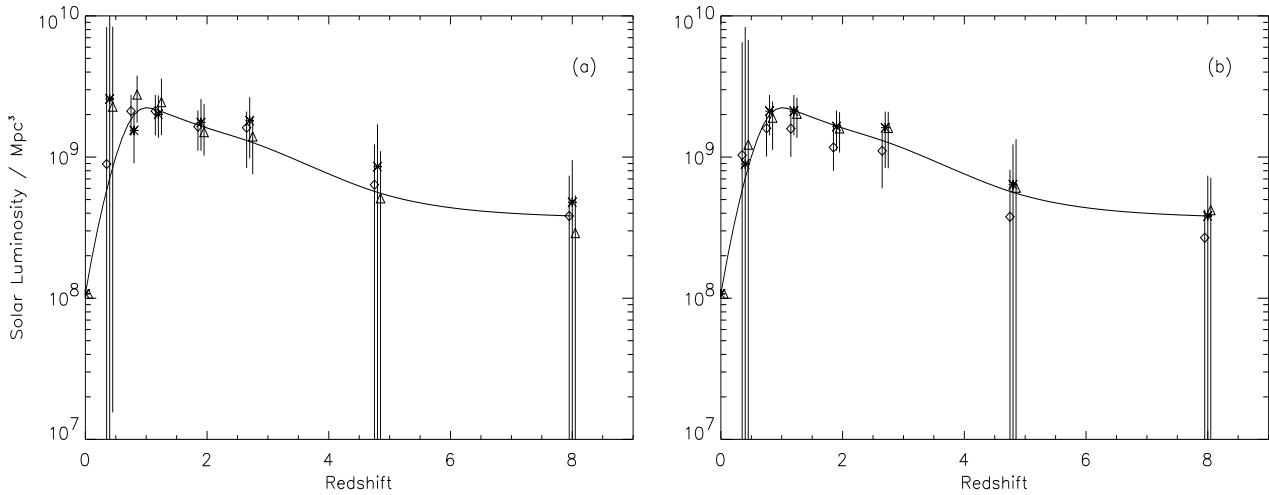


Fig. 4. Co-moving luminosity density distribution as derived from the CFIRB for different sets of parameters (with a fixed dust spectral index of 1.7). a: for a given cosmological model ($\Omega_0=0.3$, $\Omega_\Lambda=0.7$) and different luminosities (star: $3 \cdot 10^{12} L_\odot$, diamond: $5 \cdot 10^{11} L_\odot$, triangle: $7 \cdot 10^{10} L_\odot$). b: given a luminosity of $5 \cdot 10^{11} L_\odot$ and three cosmological models with $h=0.65$ (star: $\Omega_0=0.3$, $\Omega_\Lambda=0.7$, diamond: $\Omega_0=0.3$, $\Omega_\Lambda=0$, triangle: $\Omega_0=1$, $\Omega_\Lambda=0$). In each plot, points around a redshift value have been arbitrarily shifted to see the uncertainties.

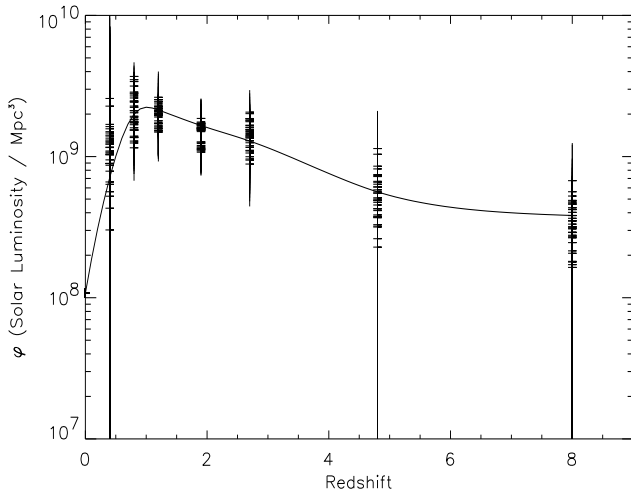


Fig. 3. Co-moving luminosity density distribution as derived from the CFIRB for all cases listed in Table 1. Also shown is the best fit passing through all cases.

we have used the CFIRB DIRBE determinations at 100, 140 and $240 \mu\text{m}$ (Lagache et al. 2000). CFIRB data points and uncertainties that are used for the determination of $\varphi(z)$ are shown in Fig. 5.

5.2. Determination of $\varphi(z)$

We determine the range of functions $\varphi(z)$ allowed by the data for each combination of SED and cosmological model. The cases used are given by the combinations of:

- Three IR galaxy luminosities ($3 \cdot 10^{12} L_\odot$, $5 \cdot 10^{11} L_\odot$ and $7 \cdot 10^{10} L_\odot$, see Fig. 2)
- Four values for the dust spectral index (1.3, 1.5, 1.7 and 2)
- Three cosmological models defined by the set of parameters h , Ω_0 and Ω_Λ ($h=0.65$, $\Omega_0=0.3$, $\Omega_\Lambda=0.7$; $h=0.65$, $\Omega_0=0.3$, $\Omega_\Lambda=0$, and $h=0.65$, $\Omega_0=1$, $\Omega_\Lambda=0$) which fix dt/dz .

To establish $\varphi(z)$ and the associated error bars we use Eq. (3). The basic algorithm for finding N_z is based on Monte Carlo simulations. N_z is sampled at a few redshift values and linearly interpolated between these values for computing the term on the right side of Eq. (3). It has been assumed that beyond $z=13$, $N_z=0$. For each case, the solution (minimum χ^2) has been obtained by exploring a wide range of randomly distributed values of N_z at each of the sampled values of z . Error bars are estimated by keeping the computed CFIRB within the uncertainties at each sampled frequency (see Fig. 5) and greater than the lower CFIRB limit at $850 \mu\text{m}$ from Barger et al. (1999). By using an iterative method for progressively reducing the range of explored values, we reach convergence for each case studied with a reasonable number of hits (~ 50000). At $z=0$, the IR production rate in the Universe is around $1.65 \cdot 10^8 h L_\odot/\text{Mpc}^3$ (Soifer & Neugebauer 1991), where h is the Hubble constant in units of 100 km/sec/Mpc^3 . This gives $\varphi(z=0) = 10^8 L_\odot/\text{Mpc}^3$ for $h=0.65$.

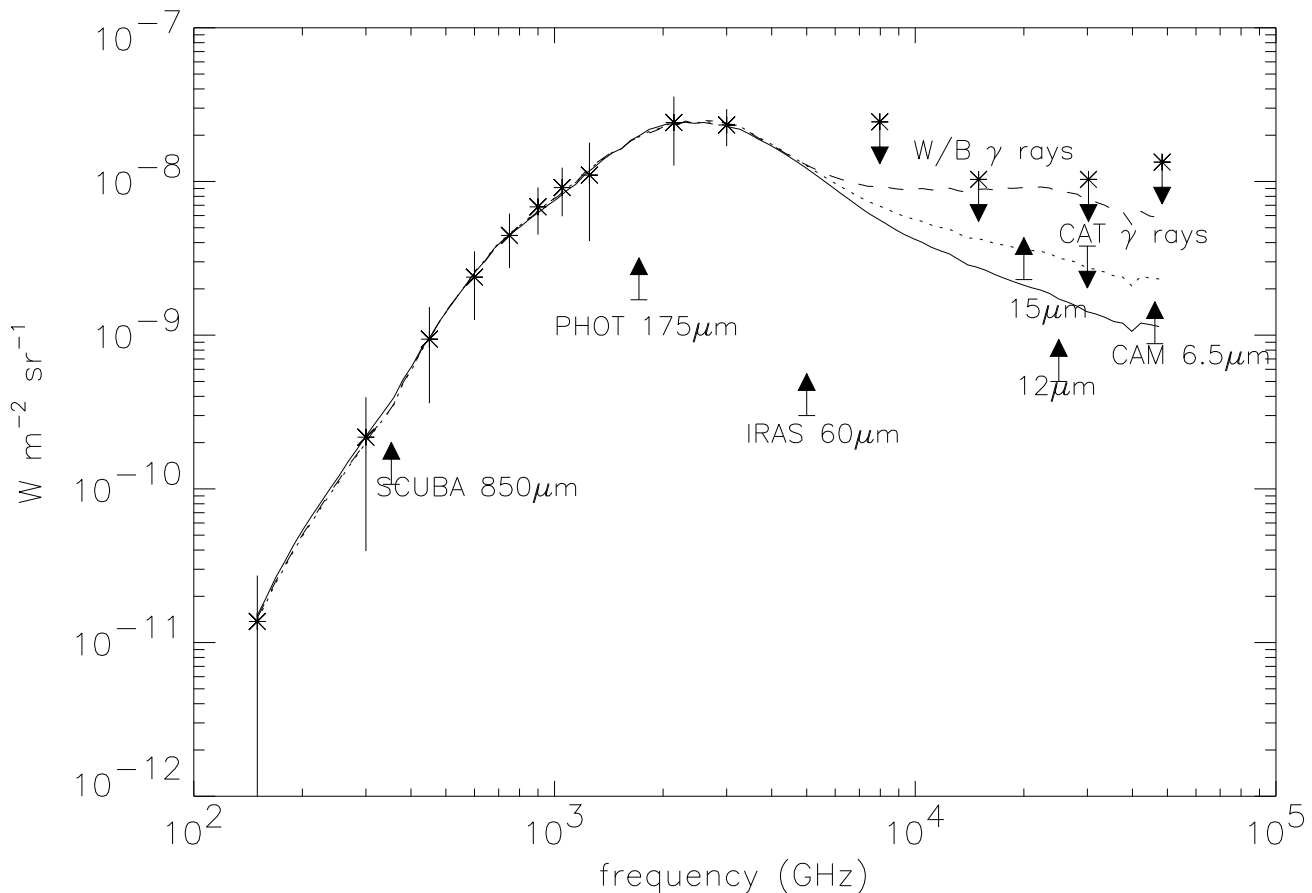


Fig. 5. CFIRB models induced from the luminosity density shown in Fig. 4a for the three luminosities (continuous line: $3 \cdot 10^{12} L_{\odot}$, dotted line: $5 \cdot 10^{10} L_{\odot}$, dashed line: $7 \cdot 10^{10} L_{\odot}$), a cosmology $h=0.65$, $\Omega_0=1$, $\Omega_{\Lambda}=0$. Also shown are the observational constraints and the CFIRB FIRAS and DIRBE spectrum (stars with error bars) computed as explained in Sect. 5.1.

5.3. Results

The results² are summarised in Table 1 for the different cosmologies and SEDs. We see that for all the considered cases, the χ^2 is very similar. This shows that, as expected, there is not a unique solution for the inversion in terms of cosmological model and average SEDs. Nevertheless the remarkable result is that there is a range of redshifts in which all acceptable solutions have the same behaviour as can be seen in Fig. 3 where the luminosity density variation, together with its uncertainties allowed by the data, is shown for each case. On the one hand, as could be expected, constraints on $\varphi(z)$ are very weak below redshift 1 (no cosmic background values at mid-IR wavelengths) and above redshift 4 (very low signal to noise ratio of the CFIRB spectrum above $800 \mu\text{m}$). On the other hand between redshifts 1 and 4, the CFIRB gives strong constraints on the history of the far-IR production rate which

cannot be established from any of the present source surveys. The luminosity density is about 10 times higher at $z=1$ than at $z=0$ and it is nearly constant up to redshift 4. Because of this rather constant behaviour, the level is only weakly dependent on the galaxy model spectrum taken with different peak wavelength (see Fig. 4) as a change in the peak wavelength mainly shifts the function $\varphi(z)$ in z . Moreover, the luminosity density in the redshift range 1 to 4 is not affected by changing the far-IR dust spectral index from 1.3 to 2. On Fig. 5 is shown the CFIRB models induced from the luminosity density variation for the three luminosities and a fixed cosmology. For the far-IR part of the spectrum, the different luminosities give automatically good fits. This is not necessarily the case below $100 \mu\text{m}$ where the result is very dependent of the galaxy model spectrum. With the present observational constraints, the best fit is obtained for a luminosity of $5 \cdot 10^{11} L_{\odot}$. This is very consistent with typical luminosities of IR galaxies that are making the background at $15 \mu\text{m}$ (Aussel, 1999).

² Figures and results can be found on G. Lagache's WEB page: <http://www.ias.fr/iasnv/people.html>

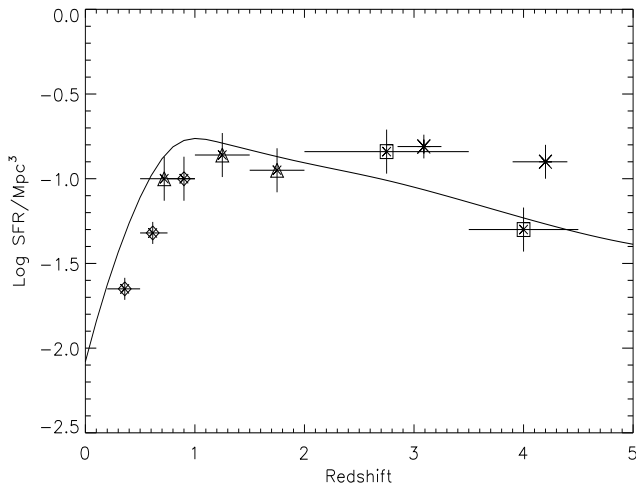


Fig. 6. SFR derived from UV/Vis/Near-IR observations (diamonds: Lilly et al. 1996; triangles: Conolly et al. 1997; squares: Madau et al. 1996 and crosses: Steidel et al. 1999) corrected for extinction by Steidel et al. (1999) and SFR derived from the CFIRB (continuous line, scaled to $H_0=50 \text{ km s}^{-1} \text{ Mpc}^{-1}$ for consistency)

Table 2. SFR (in $M_\odot \text{ yr}^{-1} \text{ Mpc}^{-3}$) deduced from the CFIRB and from deep submm SCUBA surveys (for $H_0=65 \text{ km s}^{-1} \text{ Mpc}^{-1}$).

Publications	Redshift	SFR
This paper	$z=1.9$	0.21 ± 0.10
Barger et al. 1999	$1 < z < 3$	0.25
Hughes et al. 1998	$2 < z < 4$	> 0.14

6. Cosmological implications

6.1. The star formation history of the Universe

Many models describing the evolution of galaxies including their IR and submm emission have been published in the recent years. In this section, we discuss only empirical determinations of the SFR derived from different observations.

The history of the cosmic Star Formation Rate (SFR) can be derived from deep optical surveys assuming that (1) the stellar Initial Mass function (IMF) is universal, (2) the far-UV light is proportionnal to the SFR and (3) extinction is negligible. The presence of dust which absorbs most of the UV starlight in starburst galaxies makes this last assumption highly questionable. The corrections needed to account for extinction are rather uncertain and there is much controversy about the value of this correction. Moreover, the SFR deduced from optical surveys can be underestimated if there is a significant pop-

ulation of objects so obscured that they are not detected in these surveys. A direct determination of the fraction of the stellar radiation reradiated by dust can be obtained from the IR/submm surveys if the dust enshrouded AGNs do not dominate. However, so far, the catalogues of faint submm sources with reliable redshifts are not large enough to reconstruct the history of the SFR (see Lilly et al. 1999 for a first attempt). We have shown that strong constraints can be provided by the CFIRB in the redshift range 1 to 4. It is particularly interesting to compare our determination with (1) the optically-derived SFR, corrected for extinction in the same redshift range and (2) the SFR inferred from SCUBA submm surveys. However, it is beyond the scope of this paper to discuss the cosmological implications in term of star formation. Detail discussions exist for example in Dwek et al. (1998), Pei et al. (1999), and Madau (1997).

Fig. 6 shows a compilation of the SFR derived from UV/Vis/Near-IR surveys, together with our determination of the far-IR radiation production rate history (through an interpolation). To compare the star formation rate with the luminosity density, we have to use a conversion factor. We take $\frac{SFR}{M_\odot \text{ yr}^{-1}} = \frac{L_{IR}}{7.7 \cdot 10^9 L_\odot}$ (Guiderdoni et al. 1998, with a Salpeter IMF), conversion which is in good agreement with that derived from Scoville & Young (1983) and Thronson & Telesco (1986). The UV luminosity density in Fig. 6 has been corrected for extinction by Steidel et al. (1999). We see a very good agreement between the UV and far-IR luminosity density confirming the need for a very large extinction correction. This is a strong indication that the population of galaxies that are making the submm EB (300-800 μm) seems to be the same as the population detected by Steidel et al. (1999) in their surveys of Lyman-break galaxies. This would also imply that the population of objects so obscured that they are not detected in UV/opt/near-IR surveys cannot contribute for a large fraction of the luminosity density.

Submm EB deduced SFR can also be compared to SCUBA results. Several groups are now conducting deep and ultradeep blank-field surveys (Barger et al. 1999; Hughes et al. 1998; Eales et al. 1999), that follow the first survey of Smail et al. (1997) who discover a population of luminous galaxies emitting at 850 μm amplified by lensing from foreground clusters. Two of these groups (Hughes et al. 1998; Barger et al. 1999) currently give estimates of the submm source SFR whereas Lilly et al. (1999) discuss its probable behaviour. Table 2 compares the SFR derived from the submm EB and the SCUBA determination. There is a very good agreement between the two although the SCUBA estimates should be interpreted with caution since only 20-25 % of the detected sources have secure identifications (Sanders, 1999).

Fig. 5 shows that all galaxies that are contributing to most of the background at 850 μm cannot have a luminosity

greater than $2\text{--}3 \cdot 10^{12} L_{\odot}$, standard luminosities of the current detected SCUBA sources (Lilly et al. 1999; Eales et al. 1999). This is consistent with the fact that SCUBA sources above 3 mJy account for only 20-30 % of the EB at $850 \mu\text{m}$. The present data show that the bulk of the submm EB is likely to reside in sources with $850 \mu\text{m}$ fluxes near 1 mJy. Barger et al. (1999) estimate that the FIR luminosity of a characteristic 1 mJy source is in the range $4\text{--}5 \cdot 10^{11} L_{\odot}$, which is what is expected from Fig. 5.

It can be checked that models of galaxy evolution which fit the CFIRB fall within the allowed range of SFR histories obtained here (see for example Pei et al., 1999 and Guiderdoni et al., 1998).

6.2. Redshift contribution

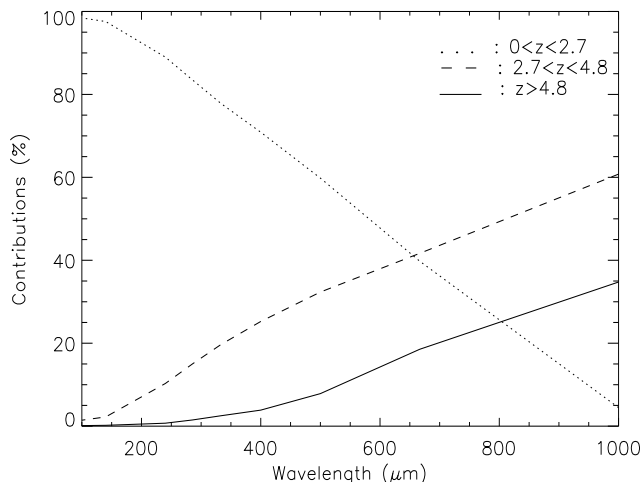


Fig. 7. Relative contribution to the CFIRB of galaxies with luminosity of $5 \cdot 10^{11} L_{\odot}$ for $z < 2.7$ (dotted line), $2.7 < z < 4.8$ (dashed line), and $z > 4.8$ (continuous line).

On Fig. 7 is shown the relative contribution from different redshift ranges to the CFIRB as a function of wavelengths (for one illustrative case $\alpha=2$, $L=5 \cdot 10^{11} L_{\odot}$, $\Omega_0=0.3$ and $\Omega_{\lambda}=0.7$). As expected, galaxies below redshift 2.7 contribute mostly at short wavelengths and galaxies above redshift 2.7 contribute mostly at long wavelength. As can be seen in Fig. 4, the small error bar at $z \sim 2.5$ shows that this conclusion is firmly established. On the contrary, the fraction shown in Fig. 7 for redshift larger than 4.8 is not well constrained by the background.

At $850 \mu\text{m}$, about 20% of the CFIRB light comes from galaxies below redshift 2.7 and 80% from above. This can be compared with the recent results of Eales et al. (1999). Their data suggest that at least 15% of the $850 \mu\text{m}$ EB is emitted at $z < 3$, which is in good agreement with what

we obtain here. However, our results show that a significant fraction of the submm EB comes from very distant objects. Such a scenario represents a picture in which a significant fraction of all stars has been formed very early in the Universe.

7. Summary

The CFIRB detected in the COBE data at wavelength greater than $100 \mu\text{m}$ contains a surprisingly large fraction of the cosmic background due to distant galaxies. The spectrum of this background at long wavelength is significantly flatter than the one observed for individual IR galaxies. This implies that the submm part of the CFIRB cannot be dominated by the emission of the galaxies which account for most of the CFIRB at $150 \mu\text{m}$, and thus contains a unique information about high redshift IR galaxies. Considering the variety of long wavelength spectra observed for these galaxies we have explored the range of possible redshift evolution histories. We show that only a co-moving production rate of far-IR radiation with strong evolution at low redshifts but little evolution between redshifts 1 and 4 is the only solution allowed by the CFIRB (the detailed low redshift evolution is much better constrained by the ISO deep surveys than by the background). Our results show that there is no evidence for a “peak” in the cosmological star formation density at $z=1\text{--}2$ as it has been assumed by many authors; it is clear that the epoch of the beginning of star formation has not yet been identified. Moreover, these results indicate that there is a divergence of the behaviour of the star formation history as compared to that of the space density of luminous AGNs (see for example Dunlop, 1997 and Shaver et al. 1998), as it was also suggested by Steidel et al. (1999).

Acknowledgements. We thanks Martin Harwit for very useful discussions on the content of this paper. The work presented here profited from very useful comments from the referee.

Appendix 1: Observational constraints on the cosmic background

At wavelengths at which the contribution is not negligible the CMB as well as its dipole distortion have been removed using the values given in Mather et al. (1994) and Fixsen et al. (1994). In the following, cosmic background is used to refer to the extragalactic electromagnetic radiation background outside the CMB.

Far-IR and submillimeter range ($\lambda \geq 100 \mu\text{m}$):

In this wavelength domain, the determination of the cosmic background has been done using the COBE FIRAS and DIRBE data. The main difficulty is to remove the bright and fluctuating Galactic dust emission. The first detection has been reported by Puget et al. (1996). They used an independent dataset (the HI 21cm survey of Hartmann et al. 1994) in addition to FIRAS spectra to remove the dust emission. The

detection of the background at $\lambda \geq 140 \mu\text{m}$ has been later confirmed by Fixsen et al. (1998), Hauser et al. (1998), Schlegel et al. (1998), Lagache et al. (1999) and Lagache et al. (2000), using the DIRBE and FIRAS data. All determinations are today in good agreement for $\lambda > 150 \mu\text{m}$. Discrepancies at $140 \mu\text{m}$ are due to different evaluations of the emission from dust associated with the ionised gas in the interstellar medium³. At $100 \mu\text{m}$, assuming an accurate subtraction of the zodiacal emission, Lagache et al. (2000) using two independent gas tracers for the HI (Leiden-Dwingeloo survey) and the H^+ (WHAM data) obtain $I_{CFIRB}(100) = 0.78 \pm 0.21 \text{ MJy/sr}$. One has to note that methods based on the intercept of the far-IR/HI correlation for the determination of the CFIRB are dangerous. For example, for the parts of the sky covered by WHAM, this intercept is about 0.91 MJy/sr , which is significantly different from the value of the CFIRB (0.78 MJy/sr). It is interesting to compare the CFIRB value of 0.78 MJy/sr to the non-isotropic residual emission found by Hauser et al. (1998). The average over three regions of the residual emission, equal to $0.73 \pm 0.20 \text{ MJy/sr}$, is in very good agreement with the Lagache et al. (2000) determination.

Mid IR range ($10 \leq \lambda \leq 80 \mu\text{m}$):

In this wavelength domain, the level of the interplanetary dust emission is very high with respect to the expected level of the cosmic background. This interplanetary dust emission peaks around $25 \mu\text{m}$. Around this wavelength, since the level of such an emission is around a thousand times the level of the background, a direct determination of the background from an earth orbit is impossible. At 25 and $60 \mu\text{m}$, our description of the interplanetary dust emission is not accurate enough to isolate the background emission. Therefore, in the Mid IR range, only indirect determinations of the background are possible. Lower limits are provided by deep cosmological surveys. We have reported on Fig. 1 lower limits derived from surveys carried out with the ISOCAM instrument aboard the IR Space Observatory: at $6.5 \mu\text{m}$ (Désert, private communication), $12 \mu\text{m}$ (Clements et al. 1999) and $15 \mu\text{m}$ (Elbaz et al. 1999). At $15 \mu\text{m}$, two values are reported: a lower limit and an absolute value. The lower limit is derived from the integrated brightness for sources above $50 \mu\text{Jy}$. As the counts flattens significantly below $100 \mu\text{Jy}$ it is interesting to display the integrated brightness down to very low fluxes using an extrapolation of the counts with a model fitting the data (Guideroni et al. 1998), as the result does not depend much on the model used. We have also reported a lower limit at $60 \mu\text{m}$ from IRAS galaxy counts (Lonsdale et al. 1990).

Upper limits are provided by the propagation of very high energy gamma rays (in the TeV range) through intergalactic space. The principle of such a determination is the following: gamma rays are absorbed by pair creation on the photons of the cosmic background. For a gamma ray of energy E coming from a distant extragalactic source all cosmic background photons with energy above a threshold $\epsilon = \frac{2m_e c^2}{E}$ will con-

tribute to the absorption of the gamma ray. As more photons contribute to the absorption when the gamma ray energy increases the gamma ray spectrum should present a curvature at high energy if the integrated density of photons is high enough. Early determinations (Stecker & De Jager, 1993; Biller et al. 1995) relied on assumptions on the shape of the spectrum at the source (a power law extrapolated from lower energies). Recently variations of the spectrum of the source Mkr 501 have been detected with CAT in a burst mode during which the X-ray emission has been observed. This allows the prediction, with minimal hypothesis, of the initial source spectrum and thus get a firm determination of an upper limit (Barrau 1998; Barrau et al, in preparation). This limit is in very good agreement with that of Funk et al. (1998) from HEGRA data. This leads to upper limits only a factor of 2 above the lower limit given by the extrapolated source counts.

Ultra-violet, visible and near-IR bands:

Pozzetti et al. (1998) have compiled number counts of extragalactic sources in the Hubble Deep Field (HDF) in the U, B, V, I and K bands. The integrated background of these counts have converged well and thus we already have a good determination of the background due to extragalactic sources. Part of the stellar radiation has been absorbed by dust and the corresponding energy has been observed in form of the IR cosmic background. Another part may have been scattered for example by intergalactic hydrogen clouds into a diffuse background. Scattering cross sections (by atoms, molecules or dust) decrease fast with wavelength thus any scattered isotropic component should be detectable primarily at ultraviolet wavelengths. Direct measurements of the extragalactic background are very difficult in the visible range because at these wavelengths, the scattered solar radiation by interplanetary particles is larger than the expected cosmic background by a factor one hundred. Fortunately in the ultraviolet the fast decrease of the solar spectrum allows a good determination of an upper limit (Bowyer 1991; Martin et al. 1991). This limit at 1500 \AA is shown in Fig. 1 and is at comparable level as the lower limit from the HDF counts in U band (at 3600 \AA). Also reported in Fig. 1 is the determination of Armand et al. (1994) which is in line of the other determinations. The Armand et al. value is based on the extrapolation of galaxy counts at 2000 \AA based on the balloon-borne experiment FOCA (Milliard et al. 1992). We thus conclude that the scattered part cannot exceed 50 % in the ultraviolet and is very likely to be negligible in the B, V, I and K bands. We can thus make the conservative hypothesis that the HDF counts provide measurements of the cosmic background. However, recent direct measurements of the optical background at 3000 , 5500 and 8000 \AA from absolute surface photometry by Bernstein et al. (in preparation, quoted by Madau & Pozzetti, 2000) lie between a factor of 2.5 to 3 higher than the integrated light from galaxy counts, with an uncertainty that is largely due to systematic rather than statistical errors. This direct determination is very difficult because of the uncertainties level of the zodiacal background to be subtracted.

Also reported in Fig. 1 are the direct estimation of the background of Dwek & Arendt (1998) with the DIRBE $3.5 \mu\text{m}$ band and Gorjian et al. (2000) at 2.2 and $3.5 \mu\text{m}$. This determination is very difficult due to the contamination by the

³ The CFIRB value of Lagache et al. (1999) is smaller than that derived in Lagache et al. (2000) since the assumed WIM (Warm Ionised gas) dust temperature was overestimated (the WIM dust spectrum was very noisy below $200 \mu\text{m}$ and the estimated dust temperature was too high).

emission of stars.

The upper limit from high energy gamma rays at 10 μm from CAT combined with the extrapolation of the integrated flux from the 15 μm counts, and the decrease of the integrated emission from sources in the ultra deep ISOCAM surveys between 15 and 6 μm , give an indication that the background spectrum must present a minimum between 3 and 10 μm . This minimum is expected to be the wavelength at which the direct stellar contribution becomes equal to the dust (in fact PAHs) emission.

Appendix 2: Far-IR radiation production rate for a single frequency emitting galaxy

If one makes the extreme assumption that the radiation of IR galaxies is concentrated at a single frequency, the spectrum of the background can be easily inverted to get the radiation production rate. If the production rate of IR radiation per co-moving volume element at a single frequency ν_o is $\phi_{\nu_o}(z)$, the resulting cosmic background in the simple case of Euclidean Universe will be given, following Eq. 2, by:

$$\frac{\phi_{\nu_o}(z)}{L_{\odot} \text{Mpc}^{-3}} = 6.5 \cdot 10^7 \frac{\nu I_{\nu}}{10^{-8} \text{Wm}^{-2} \text{sr}^{-1}} (\nu/\nu_o)^{-5/2}$$

For a simple approximation of the background with power laws

$$\nu I_{\nu} = 12 \cdot 10^{-8} (\nu/\nu_o)^{2.5} \text{Wm}^{-2} \text{sr}^{-1}$$

valid between 200 μm and 500 μm , and

$$\nu I_{\nu} = 27 \cdot 10^{-8} (\nu/\nu_o)^3 \text{Wm}^{-2} \text{sr}^{-1}$$

valid between 500 μm and 1.5 mm, ($\nu_o = 310^{12} \text{Hz}$), we deduce

$$\phi_{\nu_o}(z) = 7.8 \cdot 10^8 L_{\odot} \text{Mpc}^{-3}$$

for $1 < z < 4$ and

$$\phi_{\nu_o}(z) = 1.7 \cdot 10^9 (1+z)^{-0.5} \left(\frac{\nu_o}{310^{12} \text{Hz}} \right)^{0.5} L_{\odot} \text{Mpc}^{-3}$$

for $z > 4$.

There is *no dependance* of the energy production rate with ν_o for z between 1 and 4 because the slope of the background corresponds to the case of no evolution of the co-moving radiation production rate. This illustrates why $\varphi(z)$ does not depend very much on the spectrum of the galaxy model in this redshift range.

References

- Almaini O., Lawrence A., Boyle B.J., 1999, MNRAS 305, 59
 Armand C., Milliard B., Deharveng J.M., 1994, A&A 284, 12
 Aussel H., 1999, PhD thesis, Paris VII University
 Aussel H., Cesarsky C.J., Elbaz D., Stark J.L., 1999, A&A 342, 313
 Barrau A., 1998, PhD thesis, Paris XI University
 Barger A.J., Cowie L.L., Sanders D.B., 1999, ApJ 518, L5
 Biller S.D., Buckley J., Burdett A., et al., 1998, Phys. Rev. Lett. 80, 2992
 Biller S.D., Akerlof C.W., Buckley J., et al., 1995, ApJ 445, 227
 Bowyer S., 1991, ARAA 29, 59
 Clements C., Désert F.X., Franceschini A., et al., 1999, A&A 346, 383
 Connolly A.J., Szalay A.S., Dickinson M., et al., 1997, ApJ 486, L11
 Dunlop J., 1997, in Observational Cosmology with the New Radio Surveys, eds M. Bremer et al. (Kluwer: Dordrecht)
 Dwek E., Arendt R.G., 1998, ApJ 508, 9
 Dwek E., Arendt R.G., Hauser M.G., et al., 1998, ApJ 508, 106
 Eales S., Lilly S., Gear W.K.P., et al., 1999, ApJ 515, 518
 Elbaz D., Cesarsky C.J., Fadda D., et al., 1999, A&A 351, 37
 Fang F., Shupe D.L., Xu C., Hacking P.B., 1998, ApJ 500, 693
 Fixsen D.J., Dwek E., Mather J.C., et al. 1998, ApJ 508, 123
 Fixsen D.J., Cheng E.S., Cottingham D.A., et al. 1994, ApJ 420, 457
 Ford H.C., Tsvetanov Z.I., Ferrarese L., Jaffe, W., 1998, in IAU Symp. 184, The Central Regions of the Galaxy and Galaxies, ed. Y Sofue (Kluwer: Dordrecht)
 Funk B., Magnussen N., Meyer H. et al., 1998, Astroparticle Physics 9, 97.
 Guiderdoni B., Hivon E., Bouchet F., Maffei, B., 1998, MNRAS 295, 877
 Gorjian V., Wright E.L., Chary R.R., 2000, ApJ in press
 Hartmann D., 1994, Ph.D. thesis, University of Leiden
 Hauser M.G., Arendt R.G., Kelsall T., et al., 1998, ApJ 508, 25
 Hughes D., Serjeant S., Dunlop J., et al., 1998, Nature 394, 241
 Lagache G., Haffner L.M., Reynolds R.J., Tufte S.L., 2000, A&A 354, 247
 Lagache G., Abergel A., Boulager F., et al., 1999, A&A 344, 322
 Lilly S.J., Eales S.A., Gear W.K.P., et al., 1999, ApJ 518, 641
 Lilly S.J., Le Fèvre O., Hammer F., Crampton D., 1996, ApJ 460, L1
 Lonsdale C.J., Hacking P.B., Conrow T.P., Rowan-Robinson M., 1990, ApJ 358, 60
 Madau P., Pozzetti L., 2000, MNRAS 312, 9
 Madau P., Ferguson H., Dickinson M., et al., 1996, MNRAS 283, 1388
 Madau P., 1997, The evolution of luminous matter in the Universe, in "The Hubble deep field", Eds M. Livio, S.M. Fall, P. Madau, STScI Symposium Series
 Maffei B., 1994, PhD thesis, Paris XI University
 Martin C., Hurwitz M., Bowyer S., 1991, ApJ 379, 549
 Mather J.C., Cheng E.S., Cottingham D.A., et al. 1994, ApJ 420, 439
 Milliard B., Donas J., Laget M., et al., 1992, A&A 257, 24
 Partridge R.B., Peebble P.J.E., 1967, ApJ 148, 377
 Pei Y.C., Fall S.M., Hauser M.G., 1999, ApJ 522, 604
 Pozzetti L., Madau P., Zamorani G., et al., 1998, MNRAS 298, 1133
 Puget J.L., Lagache G., Clements D.L. et al., 1999, A&A 354, 29
 Puget J.L., Abergel A., Bernard J.P., et al., 1996, A&A 308, L5
 Sanders D.B., 1999, In Space Infrared Telescopes and Related Science, 32nd COSPAR workshop, Eds. T. Matsumoto & T. de Graauw
 Sanders D.B., Mirabel I.F., 1996, ARA&A 34, 749

- Schlegel, D.J., Finkbeiner, D.P., Davis, M. 1998, ApJ 500, 525
Scoville N.Z., Young J.S., 1983, ApJ 265, 148
Shaver P.A, Hook I.M., Jackson C.A, et al., 1998, in Highly Redshifted Radio Lines, eds C. Carilli, S. Radford, K. Menten, G. Langston
Smail I., Ivison R.J., Blain A.W., 1997, ApJ 490, L5
Soifer B.T., Neugebauer G., 1991, AJ 101, 354
Stecker F.W, De Jager O.C., 1993, ApJ 415, L71
Steidel C.C., Adelberger K.L., Giavalisco M., et al., 1999, ApJ 519, 1
Thronson H., Telesco C., 1986, ApJ 311, 98